HHS Public Access

Author manuscript

Exp Neurol. Author manuscript; available in PMC 2018 December 28.

Published in final edited form as:

Exp Neurol. 2016 September ; 283(Pt A): 39–48. doi:10.1016/j.expneurol.2016.05.018.

Lack of CAR impacts neuronal function and cerebrovascular integrity *in vivo*

Baddreddine Boussadia[a], **Giuseppe Gangarossa**[d], **Laila Mselli-Lakhal**[b], **Marie-Claude Rousset**[a], **Frederic de Bock**[a], **Frederic Lassere**[b], **Chaitali Ghosh**[e], **Jean-Marc Pascussi**[c], **Damir Janigro**[f], and **Nicola Marchi**[a,*]

[a]Laboratory of Cerebrovascular Mechanisms of Brain Disorders, Department of Neuroscience, Institute of functional Genomics, France

[b]INRA Toxalim, Toulouse, France

[c]Laboratory Signalisation, Plasticite et Cancer, Department of Cancer Biology, Institute of functional Genomics, France

[d]Center for Interdisciplinary Research in Biology (CIRB), College de France, Paris, France

[e]Cerebrovascular Research, Lerner Research Institute, Cleveland Clinic, USA

[f]Flocel Inc., Cleveland, OH, USA

Abstract

Nuclear receptors (NRs) are a group of transcription factors emerging as players in normal and pathological CNS development. Clinically, an association between the constitutive androstane NR (CAR) and cognitive impairment was proposed, however never experimentally investigated. We wished to test the hypothesis that the impact of CAR on neurophysiology and behavior is underlined by cerebrovascular-neuronal modifications. We have used $CAR^{-/-}$ C57BL/6 and wild type mice and performed a battery of behavioral tests (recognition, memory, motor coordination, learning and anxiety) as well as longitudinal video-electroencephalographic recordings (EEG). Brain cell morphology was assessed using 2-photon or electron microscopy and fluorescent immunohistochemistry.

We observed recognition memory impairment and increased anxiety-like behavior in $CAR^{-/-}$ mice, while loco-motor activity was not affected. Concomitantly to memory deficits, EEG monitoring revealed a decrease in 3.5–7 Hz waves during the awake/exploration and sleep periods. Behavioral and EEG abnormalities in $CAR^{-/-}$ mice mirrored structural changes, including tortuous fronto-parietal penetrating vessels. At the cellular level we found reduced ZO-1, but not CLDN5, tight junction protein expression in cortical and hippocampal isolated microvessel preparations. Interestingly, the neurotoxin kainic acid, when injected peripherally, provoked a rapid onset of generalized convulsions in $CAR^{-/-}$ as compared to WT mice, supporting the hypothesis of vascular permeability. The morphological phenotype of $CAR^{-/-}$ mice also included

*Corresponding author at: Cerebrovascular Mechanisms of Brain Disorders, Institut de Génomique Fonctionnelle, CNRS UMR5203, INSERM U1191, Université Montpellier, 141 Rue de la Cardonille, 34094 Montpellier Cedex 5, France. nicola.marchi@igf.cnrs.fr (N. Marchi).

Supplementary data to this article can be found online at http://dx.doi.org/10.1016/j.expneurol.2016.05.018.

some modifications of GFAP/IBA1 glial cells in the parenchymal or adjacent to collagen-IV^{+} or FITC^{+} microvessels. Neuronal defects were also observed including increased cortical NEUN^{+} cell density, hippocampal granule cell dispersion and increased NPY immunoreactivity in the CA1 region in CAR$^{-/-}$ mice. The latter may contribute to the *in vivo* phenotype.

Our results indicate that behavioral and electroencephalographic changes in adult CAR$^{-/-}$ mice are concomitant to discrete developmental or structural brain defects. The latter could increase the vulnerability to neurotoxins. The possibility that interfering with nuclear receptors during development could contribute to adulthood brain changes is proposed.

Keywords

Development; Cerebrovascular; Nuclear receptors; Memory; Stress

1. Introduction

Nuclear receptors (NRs) are a superfamily of transcription factors. Recent evidence is expanding the breadth of NR functions to include a role in brain cortical development (Fan et al., 2008), memory formation (Hawk et al., 2012; Kaur and Sodhi, 2015; Yang and Wang, 2014), anxiety (Tan et al., 2012), vascular or barrier integrity and tissue homeostasis (Banerjee et al., 2015; Ogura et al., 2012; Venkatesh et al., 2014; Wang et al., 2014; Zhao and Bruemmer, 2010; Zhao et al., 2010). Among the existing NR, xenobiotic receptors, such as the Pregnane X Receptor (NR1I2) and the Constitutive Androstane Receptor (CAR, NR1I3), are sensors of toxic byproducts (Tolson and Wang, 2010). Experimental evidence supports a functional impact of a NR1I2 receptor in memory function in mice (Kaur and Sodhi, 2015). Interestingly, regulation of vascular inflammation and mechanisms of homeostasis were shown to encompass pathways controlled by NR (Banerjee et al., 2015; Wang et al., 2014; Zhao and Bruemmer, 2010; Zhao et al., 2010). Moreover, loss of NR1I2 receptor was associated with a disrupted gastro-intestinal barrier and decreased tight junction levels resulting in increased susceptibility to systemic toxic insults (Venkatesh et al., 2014).

No studies have investigated whether loss of CAR may impact neuronal functions *in vivo*. The latter is clinically relevant as a missense CAR mutation was reported in patients presenting with intellectual disability and comorbidities including spontaneous seizures (Kleefstra et al., 2012). It is unknown whether, and consistent with CAR ablation, cellular brain changes exist in the adulthood, including vascular barrier modifications (Venkatesh et al., 2014; Wang et al., 2014). Remarkably, experimental and clinical evidence demonstrated cerebrovascular damage as an etiological player involved in brain diseases, including psychiatric illness (Khandaker et al., 2015), seizure onset and progression (Friedman, 2011; Marchi et al., 2007, 2012; van Vliet et al., 2014), and cognitive decline (Abbott et al., 2006; Obermeier et al., 2013; Snyder et al., 2015; Zhao et al., 2015). Both developmental or acquired pathological factors can affect cerebrovascular permeability or the inflamma-tory basal state, thus perturbing brain homeostasis and the neurophysiology of the adult brain (Obermeier et al., 2013).

Xenobiotic receptors are functionally expressed in the brain, as demonstrated by the modulation of specific downstream gene targets (Bauer et al., 2006; Wang et al., 2010). We therefore tested the hypothesis that genetic ablation of CAR is associated with modifications of basal *in vivo* neuronal functions in the adult brain (Dai et al., 2012; Fan et al., 2008; Hawk et al., 2012; Kaur and Sodhi, 2015; Tan et al., 2012). We also evaluated whether neuro-vascular morphological changes exist in $CAR^{-/-}$ brains concomitant to *in vivo* functional modifications. The possible contribution of CAR to brain maldevelopmental or homeostatic mechanisms is discussed.

2. Materials and methods

2.1. Animals

All experiments followed European Union (Council directive 86/609EEC) and institutional guidelines for laboratory animals care and use. Mice were hosted at the IGF or INRA animal facilities (institutional license approved by the French Ministry of Agriculture No. D34–172-13 and B31–555013). Mice were housed on a 12 h light-dark cycle with food and water *ad libitum*. The animal experiment protocols were approved by the local ethical committee for animal testing (05185.01 and 00846.01). $CAR^{-/-}$ mice and wild type on a C57BL/6j genetic background (Wei et al., 2000) were originally established and previously used by the authors of this manuscript (INRA, see (Roques et al., 2013)). Colony founders were provided to LK (INRA) by Pr. Urs A Meyer (Biozentrum, University of Basel, Switzerland). We used adult male mice (8–12 weeks old).

2.2. Behavioral studies

A total of n = 12 $CAR^{-/-}$ and n = 12 WT mice were used for behavioral testing (see Figs. 1 and 2).

2.2.1. Spatial object recognition—The spatial object recognition test was performed as previously described (Gangarossa et al., 2014a, 2014b). Briefly, mice were habituated to the experimental arena for 10 min. The following day, mice were allowed to freely explore 2 different objects (A and B) located in the same site of the arena. Object interaction was defined as approaching the object with the nose (1 cm). Following a retention interval of 24 h, mice underwent a 5 min recall session when the arena contained one of the two objects displaced in the other site (novel place). Following each session, the objects and the open field were cleaned with 70% ethanol. The experiments were videotaped and the time spent exploring the objects was scored. The percentage of exploration time was calculated as % exploration = ((Time B) / (Time A + Time B)) ∗ 100.

2.2.2. Rotarod test—Balance and motor coordination as well as motor learning were assessed using an accelerating rotarod (Ugo Basile, Comerio, Italy) as previously described (Gangarossa et al., 2014a, 2014b). Mice were placed on the rotating drum accelerating from 4 to 40 rpm over 5 min for 3 trials a day and for 3 consecutive days. The trial interval was 45 min for all mice. Rotarod sessions were scored for latency to fall or ride around the rod.

2.2.3. Spontaneous locomotor activity—Locomotor activity was measured as previously described (Gangarossa et al., 2014a, 2014b). Horizontal and vertical activities were measured in a circular corridor (Imetronic, Pessac, France). Counts for horizontal activity were incremented by consecutive interruption of two adjacent beams placed at a height of 1 cm per 90° sector of the corridor (mice moving through one-quarter of the circular corridor) and counts for vertical activity (rearing) as interruption of beams placed at a height of 7.5 cm along the corridor (mice stretching upwards).

2.2.4. Elevated-plus maze (EPM)—The elevated plus maze was elevated 1 m above the floor (black plastic with 2 open arms 5 cm width × 35 cm length × 0.5 cm height; 2 closed arms 5 width × 35 cm length × 15 cm height). Mice were placed in the center of maze facing one of the open arms and were allowed to explore the maze for 10 min. Experiments were videotaped and scored for entries and time spent in the closed arms (4 paws within) or open arms (4 paws within).

2.2.5. Open field—Spontaneous exploratory behavior was monitored in an open field (white plastic arena with 35 cm width × 50 cm length × 20 cm height) for 10 min. The center zone was defined as a virtual perimeter within 5 cm from the sides of the arena. Experiments were videotaped and an observer scored the time spent in the center (4 paws inside the center zone) and the number of transitions in the center zone.

2.3. Video-encephalography and signal analysis

2.3.1. Baseline EEG and frequency analyses—n = 4 $CAR^{-/-}$ C57/BL6j and n = 4 WT mice were implanted in the fronto-parietal cortex and were used to characterize baseline EEG activity. Each mouse was monitored using video-EEG for a total of 50 h (50% night and 50% day) over a period of 1 week. EEG signals were acquired at 200–600 Hz – stored and analyzed using Neuroscore and MatLab. Ten minutes EEG samples were extracted from all recordings and: i) classi-fied as day or night; ii) separated by awake/exploratory vs sleep (Video); iii) video analysis ruled out motion artifacts associated with scratching, eating, drinking or chewing. As a result we obtained the following number of EEG extracts: n = 39 WT awake/exploratory, n = 43 WT sleep, n = 34 $CAR^{-/-}$ awake/exploratory and n = 31 $CAR^{-/-}$ sleep. The latter corresponded to the EEG time: 390 min WT awake/exploratory, 430 min WT sleep, 340 min $CAR^{-/-}$ awake/exploratory and 310 min $CAR^{-/-}$ sleep. All EEG samples were processed using Neuroscore (Periodogram Power Bands; epoch duration 10 s) to calculate the relative value (0–100%) within each 0.5 Hz increments (0.5–30 Hz).

2.3.2. Kainic acid injection—A total of n = 16 $CAR^{-/-}$ C57/BL6j and n = 16 C57/BL6j WT mice were used for video-EEG or Racine behavioral monitoring of status epilepticus (SE) induced using i.p. kainic acid (KA, 25 mg/kg; stock solution 10 mg/ml KA in PBS, pH = 7). In particular, n = 7 $CAR^{-/-}$ C57/BL6j and n = 7 C57/BL6j WT mice were implanted with fronto-parietal cortical electrodes and EEG recordings. Mice were monitored up to 24 h after KA. The following endpoints were determined: i) number of mice developing SE; ii) time of SE onset; iii) time spent in generalized SE normalized by the total duration of each EEG recording (from KA injection to death or up to 5 h to follow SE onset and evolution). Briefly, mice were anesthetized with ketamine/xylazine, placed on a

stereotaxic frame and the skull exposed. A preamplifier (2 differential channels, Pinnacle Inc., USA) was connected to EEG leads. Mice were left unrestrained for one week.

2.3.3. CINPA1 injections—A cohort of male adult C57/BL6j WT mice (n = 3) was repetitively injected with CINPA1 (5605, Tocris Bioscience), a novel and potent CAR antagonist exhibiting high selectivity for CAR over other xenobiotic NR1I (Cherian et al., 2015a, 2015b). CINPA1 has low molecular weight (395 Da) and it is lipophilic (LogP > 3), therefore penetrating cell membranes (Cherian et al., 2015a, 2015b). A dose response was performed (1 mg/kg, 10 mg/kg and 50 mg/kg) based on available IC_{50} (Cherian et al., 2015a, 2015b). Video-EEG was recorded for 24 h following each injection. Control group refers to video-EEG (12 to 24 h) recorded before CINPA1 injections in each animal. Video-EEG data were sorted and extracted as described above (see Supplemental Table 1). The following number of EEG extracts (5 minutes each) were analyzed: n = 31 awake/exploration and n = 33 sleep (control); n = 52 awake/exploration and n = 87 sleep (1 mg/kg CINPA1); n = 63 awake/exploration and n = 97 sleep (10 mg/kg CINPA1).

2.4. Microvessel isolation, western blot and quantifications

2.4.1. Capillary isolation—We performed 2 separate experiments (i and ii) pulling together the cortical and hippocampal preparations obtained from: i) n = 5 $CAR^{-/-}$ and n = 5 WT; ii) n = 6 $CAR^{-/-}$ and n = 6 WT mice (see Fig. 4). The latter was implemented to obtain a sufficient protein yield, amenable for subsequent western blot analysis. A detailed procedure is described in Shawahna et al. (2011). Briefly, white matter, meninges, midbrain, choroid plexus, and olfactory lobes were removed from the brains and the remaining tissue (hippocampi and cortices) homogenized. Tissue was kept in cold PBS (2.7 mM KCl, 1.5 mM KH_2PO_4, 136.9 mM NaCl, 8.1 mM Na_2HPO_4, 1 mM $CaCl_2$, 0.5 mM $MgCl_2$, 5 mM D-glucose, and 1 mM sodium pyruvate) throughout the isolation procedure. An aliquot of 30% Ficoll was added to an equal volume of brain homogenate and capillaries were separated from the parenchyma by centrifuging at 5800g for 20 min. Capillaries were isolated using selective filtrations (>20 μm and <100 μm).

2.4.2. Whole brain tissues—Briefly, cortical, and hippocampal tissues were homogenized using a buffer containing 0.1% sodium dodecyl sulfate (SDS), protease inhibitor cocktail (Promega, Madison, WI, USA), 50 mM Tris–HCl (pH 7.4), 10 mM EDTA, 1 mM Na_3VO_4, 40 mM sodium pyrophosphate, 50 mM NaF, and 1 mM dithiothreitol (DTT). Samples where then centrifuged (12,000 rpm for 10 min) and protein content quantified.

2.4.3. Western blots—Samples were separated by electrophoresis and then transferred onto a nitrocellulose membrane. After 1 h of blocking in skimmed milk, the membranes were probed overnight at 4 °C with a mouse anti-Zona Occludens 1 (1:400; 339100, Invitrogen), mouse anti-Claudin 5 (1:800; 352500, Invitrogen) or mouse anti-Actin (1:10,000; ab6276, Abcam). Secondary goat anti-mouse horseradish peroxidase (HRP)-conjugated (1:4000) antibody was used. Relative band densities were measured and normalized using ImageJ. WB bands obtained using isolated microvessels (Fig. 4D) are not quantified as they represent tissue mean signals of i) n = 5 and ii) n = 6 mice/group.

2.5. Transparent SeeDB brain, electron microscopy and immunohistochemistry

Transparent brain preparation was performed on $CAR^{-/-}$ and WT mice following the procedures described by Ke et al. (2013). Briefly, mice were perfused intracardially using a 25 mg/ml solution of FITC-albumin (300 μl/mouse). The fronto-parietal cortices were isolated, treated using the SeeDB protocol (Ke et al., 2013) and analyzed using 2-photon microscopy (see Fig. 4A and Supplemental Movies 1–2). Electron microscopy was performed at the Core Facility (University of Montpellier, France) from hippocampal and cortical blocks.

2.5.1. Tight junctions—A total of n = 6 WT and n = 6 $CAR^{-/-}$ mice were used specifically for this immunohistochemistry. After perfusion with PBS mice brains were dissected and immerged in sucrose 30%. Brains were then snap frozen and stored at −80 °C. Slices (20 μm) were obtained using a cryostat. Slices were post-fixed directly on the slide using methanol/acetone (v/v 50/50) at −20 °C and immerged in the solution for 1 min. Immunohistochemistry was performed after PBS washes. Slices were added with blocking solution (PBS, triton 0.3%, goat or horse serum depending on the secondary antibody used) for 1 h at 4 °C. Primary antibody was diluted in blocking solution (Z01 or CLDN5, see Supplemental Table 2) overnight at 4 °C. After PBS washes, secondary antibody was added in PBS (1:2000, donkey anti-rabbit Cy3, Jackson Immunoresearch 711–165-152) for 2 h at room temperature. Slices were mounted using moviol.

2.5.2. Neuro-peptide Y—Immunostaining was performed of PFA 4% fixed brains. Slices (30 μm) were cut using a vibratome and stored in cryoprotectant solution at −20 °C. Free floating slices were rinsed using PBS and blocking solution (PBS, BSA 2%, triton 0.25% and horse or goat serum 3%) added for 2 h at room temperature. Primary antibody (anti-NPY see Supplemental Table 2) was added for 36 h at 4 °C. After PBS washed, secondary antibody (1:2000, donkey anti-rabbit Cy3, Jackson Immunoresearch 711–165-152) was added (PBS + triton 0.25%).

2.5.3. Collagen IV—Basal lamina was stained using Collagen IV (polyclonal rabbit anti-collagen IV antibody, ab6586, 1:100, Abcam). Staining was performed using an antigen retrieval technique based on citrate buffer (pH = 6).

2.5.4. GFAP/IBA1 inflammation—PFA fixed brain slices were incubated with blocking solution (PBS, triton 0.25% and horse serum 20%) for 1 h at room temperature. Primary antibodies were then added in PBS (see Supplemental Table 2) overnight at 4 °C. After PBS washes, secondary antibodies were added (1:2000, donkey anti-rabbit Cy3, Jackson Immunoresearch 711–165-152 for IBA1; donkey anti-mouse Jackson 715–165-151 for GFAP and NEUN). For triple immunohistochemistry (Fig. 5A-A1) a goat anti-mouse Alexafluor 350 was used for GFAP (see Supplemental Table 2).

2.6. Statistics

Data were analyzed using one-way or two-way ANOVA followed by Bonferroni post hoc test. $F_{(x, y)}$ indicates cumulative distribution and degree of freedom (Prism). Student's *t*-test with equal variances was used for groups of 2, when relevant. In all cases, significance

threshold was set at $P < 0.05$. Statistical analyses were performed using GraphPad Prism 5.0 (GraphPad Prism Software Inc., San Diego, USA) or Origin Microcal.

3. Results

3.1. Impaired memory function and increased anxiety in CAR$^{-/-}$ mice

We performed a battery of behavioral tests investigating whether CAR ablation may impact memory, learning and anxiety. We measured the integrity of recognition and motor/procedural memory processes. In the object place recognition test CAR$^{-/-}$ mice did not show preference for the familiar or relocated object during the recall session (24 h after exploratory phase) as opposed to WT mice (Fig. 1A and B). This was not due to an impairment of the exploratory drive since exploration of the two objects was not affected in CAR mice during the familiarization phase (data not shown). Motor skill learning was also assessed using the accelerating rotarod. No differences were observed during the first day of training, suggesting unaltered motor function and coordination in CAR$^{-/-}$ mice (Fig. 1C). Interestingly, CAR$^{-/-}$ mice showed a decreased improvement of rotarod motor performance compared to WT (Fig. 1C–D); this is consistent with decreased learning ability. Thus, all mice gradually acquired motor skills following prolonged training, even though the learning index was higher in WT as compared to CAR$^{-/-}$ mice (3 days; Fig. 1C and D). No differences in the spontaneous horizontal (Fig. 1E-E1) and vertical activity (Fig. 1F-F1) were observed in CAR$^{-/-}$ mice. Our results suggest a link between lack of CAR and memory or learning performances, although sparing locomotor coordination and activity.

Anxiety-like behavior was also observed in CAR$^{-/-}$ mice; this was evaluated by the elevated plus maze (EPM) and the open field tests (Fig. 2). In the EPM test, CAR$^{-/-}$ mice spent less time in the open arms as compared to WT mice. Differences were observed in the number of entries in both closed and open arms. We further measured the spontaneous behavior using the open field test (novel and stressful environment; Fig. 2D–E). CAR$^{-/-}$ mice spent less time and had a reduced number of transitions in the center of the field as compared to WT, indicating increased anxiety (Fig. 2). These results indicate a link between deletion of the nuclear receptor CAR and anxiety-like behaviors in the adulthood.

3.2. Constitutive decrease of 3.5–7 Hz activity in CAR$^{-/-}$ mice in vivo

We performed a longitudinal video-EEG study to test whether the observed behavioral changes were associated with abnormal electrographic activity (Chauviere et al., 2009). Compared to WT, CAR$^{-/-}$ mice displayed a constitutive reduction in relative 3.5–7 Hz power during sleep and awake/exploratory states. Fig. 3A–B shows examples (10 min) of EEG recordings during awake/exploratory or sleep periods and relative frequency abundances (uV^2; 0–30 Hz). Data relative to CAR$^{-/-}$ and WT mice (50 h video-EEG recordings each mouse; see Section 2 for details) are shown in Fig. 3C (means ± SD). Note that the contribution of 3.5–7 Hz waves was decreased in CAR$^{-/-}$ mice. Fig. 3D-D1 details the changes in activity in CAR$^{-/-}$ mice observed during awake/exploratory and sleep stages. Data were obtained using the following cumulative EEG durations: 390 min WT awake/exploratory, 430 min WT sleep, 340 min CAR$^{-/-}$ awake/exploratory and 310 min CAR$^{-/-}$

sleep. All data are pulled together in Fig. 3E-E1. Changes in EEG activity in $CAR^{-/-}$ mice are consistent with memory deficits (Fig. 1; see also (Chauviere et al., 2009)).

3.3. Cerebrovascular and parenchymal cells changes in $CAR^{-/-}$ mice

Loss of the xenobiotic receptor NR1I2 has been associated with altered barrier function in peripheral organs (Venkatesh et al., 2014). We tested the hypothesis that, when CAR is deleted, congenital cerebrovascular changes are concomitant to the behavioral and EEG modifications. Cerebrovascular dysfunction underlies changes in neuronal activity in brain diseases as demonstrated in human and experimental models (Khandaker et al., 2015; Marchi et al., 2014). Using a transparent brain preparation and 2-photon reconstruction we found the presence of truncated penetrating cortical vessels in $CAR^{-/-}$ mice (Fig. 4A-A1 and Supplemental Movies 1 and 2). Only sporadic and point form FITC-Dextran leakages (10 kDa) were observed in $CAR^{-/-}$ mice (Fig. 4B4 and D). At the molecular level, we quantified the expression of the tight junctions ZO1 and CLDN5 proteins in brain homogenates (Fig. 4C) or in microvessels isolated from hippocampi and fronto-parietal cortices (Fig. 4E). While no significant changes in CLND5 expression were observed, ZO1 levels were reduced in $CAR^{-/-}$ mice. Immunohistochemistry indicate distinct perivascular regions of discontinuous ZO1 lining the $FITC^{+}$ microvessels (Fig. 4D-D1) in $CAR^{-/-}$ mice.

Vascular modifications were accompanied with discreet changes in neuronal architecture. The latter included an increased fronto-parietal cortical NEUN density (Supplemental Fig. 2A-A1 and D-D3) and dispersion of hippocampal granule cells in $CAR^{-/-}$ mice (Supplemental Fig. 2B−C). In addition, staining with the neurotransmitter neuropeptide Y (NPY) was increased in CA1 pyramidal interneurons (Supplemental Fig. 2E–F). Interestingly, changes in brain neuronal architecture were also reported in other NR deficient mice (Fan et al., 2008). The latter is consistent with impaired neuronal functional (Thorsell et al., 2000, 2006).

We also found signs of $GFAP^{+}$ astrocytes and IBA^{+} microglial cells morphological abnormalities in $CAR^{-/-}$ mice. In $CAR^{-/-}$ mice hippocampal astrocytes presented with dishomogenous morphology and irregular perivascular distribution as compared to WT where astrocytes were uniformly arranged (Fig. 5A–B). $GFAP^{+}$ cell rarefication was observed in $CAR^{-/-}$ mice. Quantification of total GFAP fluorescence indicated no significant changes between WT and $CAR^{-/-}$ mice (data not shown) (Wilhelmsson et al., 2006). IBA^{+} microglia displayed increased cell body size and a trend increase of microglial-microvascular contacts in $CAR^{-/-}$ mice (Fig. 5C–E). Interestingly, the total number of IBA^{+} cells was decreased in $CAR^{-/-}$ as compared to WT. Analysis of microvessels using electron microscopy indicated localized micro-morphological changes consistent with signs of microvascular inflammation (Fig. 5F–G) in $CAR^{-/-}$ mice. Our results are in accordance with a role of NR in inflammatory vascular reactivity (Ogura et al., 2012; Zhao and Bruemmer, 2010; Zhao et al., 2010).

3.4. $CAR^{-/-}$ mice are susceptible to neurotoxins

We then tested the hypothesis that morphological changes observed in $CAR^{-/-}$ mice are associated with increased susceptibly to systemically injected neurotoxins (kainic acid; KA).

$CAR^{-/-}$ mice developed generalized status epilepticus (SE) more rapidly as compared to WT (Fig. 6A–B). $CAR^{-/-}$ mice also experienced longer SE episodes (Fig. 6C). Although only an indirect association can be hypothesized, a more severe seizure outcome could be sustained by the cellular changes described in Figs. 4–5 and Supplemental Figs. 1–2. Changes in vascular permeability may favor passage of systemically circulating neurotoxins. The latter is in accordance with Fan et al. (2008), Hawk et al. (2012), Kaur and Sodhi (2015), Kleefstra et al. (2012), Tan et al. (2012), and Venkatesh et al. (2014) and a role of NR in barrier homeostasis (Venkatesh et al., 2014; Wang et al., 2014).

4. Discussion

We report an unexplored role of the nuclear receptor CAR in brain pathophysiology. The phenotype associated with loss of CAR in mice endorses future studies on the cellular mechanisms underlying memory deficits and anxiety-like behavior in the absence of NR as well as the potential role of CAR during development. Interestingly, a recent clinical study identified an uncharacterized missense mutant of CAR in subjects affected by intellectual disabilities (Kleefstra et al., 2012). However, significant differences exist between the human data and our experimental approach, as in our study we used CAR knockout mice. CAR might have both genomic and non-genomic function, resulting in dissimilar functional outcomes.

Our results bear clinical significance as a number of xenobiotic and environmental toxins, including pesticides, modulate CAR activity (Banerjee et al., 2015; Wei et al., 2000). Activation or inhibition of CAR occurring during the gestation period could promote developmental changes impacting basal functions in the adult brain. We found signs of constitutive cerebrovascular barrier dysfunctions and parenchymal changes possibly reflecting homeostatic modifications (Wilhelmsson et al., 2006). The latter is clinically relevant as the association between cerebrovascular permeability, the immune system and neuronal dysfunction is gaining momentum (Friedman, 2011; Khandaker et al., 2015; Marchi et al., 2014). Thus, loss of cerebrovascular integrity impacts cognition, affection (Falcone et al., 2015; Khandaker et al., 2015), behavior and susceptibility to seizures (Friedman, 2011; Khandaker et al., 2015; Marchi et al., 2014). Recent studies indicated neuronal maldevelopment (Fan et al., 2008) and changes in neuronal metabolism of neurotransmitters in NR deficient mice (Huang et al., 2015; Tan et al., 2012) including PXR, the CAR cognate xenobiotic receptor (Frye et al., 2013; Zhou et al., 2009).

4.1. CAR loss and behavioral-electroencephalographic changes in the adult brain

We show agreement between behavioral results and EEG recordings, pointing to a link between loss of CAR and memory deficits. The decreased of the 3.5–7 Hz EEG component during sleep and awake/exploration could be a neurophysiological substrate of memory impairment (Chauviere et al., 2009). Lack of CAR was also associated with increased anxiety scores while no changes in locomotor activity were detected. Our results indicate a localized increased of hippocampal NPY in $CAR^{-/-}$ mice. Interestingly, increased NPY expression has been associated to impaired spatial learning in mice (Thorsell et al., 2000, 2006). The impact of CAR in brain development is further supported by initial data obtained

using a cohort of adult WT mice treated with the specific CAR antagonist CINPA1 (Cherian et al., 2015a, 2015b). Our initial results (Supplemental Table 1) indicate that CINPA1 did not recapitulate the EEG phenotype observed in $CAR^{-/-}$ mice. Thus, at dosage of 1 and 10 mg/kg CINPA1 did not provoke consistent changes in the EEG frequency spectra. (see Supplemental Table 1). Video review showed that, at these dosages, CINPA1 did not significantly alter the awake/sleep cycles and pattern, while 50 mg/kg did. The fact that CINPA1 in adult WT mice did not mimic the EEG phenotype observed in $CAR^{-/-}$ could reflect the difference between pharmacologic inhibition of CAR transcriptional activity and the genetic absence of the entire CAR protein or even developmental changes associated with the lack of this NR.

The developmental role of CAR expression follows evidences obtained for other NR (Fan et al., 2008; Hawk et al., 2012; Tan et al., 2010, 2012). Our behavioral read-out shares similarities with other NR deficiencies, including ablation of X liver receptor (Tan et al., 2012) and the NR4A (Hawk et al., 2012). It was also suggested that PXR plays a role in memory performance (Huang et al., 2015; Kaur and Sodhi, 2015). Changes in neuro-steroid levels were proposed as a mechanism contributing to behavioral changes via xenobiotic NR modulation (Frye et al., 2013). The homeostasis of multiple neurotransmitters is altered in Farnesoid X receptor deficient mice (Huang et al., 2015). It remains to be investigated whether these mechanisms apply to loss of CAR.

4.2. Do NRs control developmental barrier integrity?

CAR is involved in a plethora of cellular functions extending beyond its classic role in controlling downstream metabolic enzymes (Yang and Wang, 2014). Lack of PXR, a cognate CAR receptor, is associated with gastro-intestinal barrier permeability and reduced tight junction protein levels (Venkatesh et al., 2014). This indirectly supports our results since peripheral and CNS barrier have overlapping molecular machinery controlling paracellular permeability. We report decreased microvascular ZO1 expression in $CAR^{-/-}$ mice. As reported for peripheral barriers (Venkatesh et al., 2014), increase permeability could constitute a risk factors for xenotoxicity. Overwhelming experimental and clinical evidences indicate that loss of BBB-mediated CNS homeostasis is a recognized etiological factor in behavioral and seizure disorders (Falcone et al., 2015; Khandaker et al., 2015; Marchi et al., 2012; Snyder et al., 2015). Our results are in agreement with this evidence showing a rapid onset of status epilepticus following intra-peritoneal injection of a prototype pro-convulsant toxin in $CAR^{-/-}$ mice.

Nuclear receptors are also implicated in peripheral organ hypertrophy (Ross et al., 2010), cell growth or differentiation, including tumors, (Chakraborty et al., 2011) and barrier structure (Venkatesh et al., 2014). Interestingly, altered radial glia architecture was reported in the absence of NR, which may explain an abnormal neuro-vascular development (Fan et al., 2008; Tan et al., 2010). Negative NR modulation could promotes activation of pro-inflammatory pathways and a defective neurovascular homeostasis (Banerjee et al., 2015; Venkatesh et al., 2014; Wang et al., 2014; Zhao and Bruemmer, 2010; Zhou et al., 2009). It remains to be elucidated whether these effects are linked to cerebrovascular permeability, neuronal dysfunction or both.

4.3. Final remarks

Accumulating evidence support a link between NR and inflammatory processes (Ogura et al., 2012; Venkatesh et al., 2014; Zhao and Bruemmer, 2010; Zhou et al., 2009). Specific evidence connects nuclear receptors to endothelial cell proliferation (Zhao and Bruemmer, 2010). Inflammatory processes also include mechanisms of monocyte recruitment to the vascular wall under the control of NR (Zhao et al., 2010). PXR was demonstrated to be sensitive to changes in flow and hemodynamics, impacting the expression of detoxification genes in vascular endothelial cells (Wang et al., 2013). Mice deficient for PXR displayed over-expression of NF-κB target genes in multiple tissues accompanied by intestinal inflammation. NF-κB modulation impact NR activity and the expression of its target genes (Zhou et al., 2009). A link between NR and pro-inflammatory cytokines was also reported. Finally, gene array data indicate increased genes linked to cell proliferation, including extracellular matrix, in the absence of CAR (Li et al., 2015).

Our results introduce CAR among the xenobiotic nuclear receptors possibly involved in neuro-vascular pathology (Fan et al., 2008; Frye et al., 2013; Hawk et al., 2012; Huang et al., 2015; Kaur and Sodhi, 2015; Litwa et al., 2015; Tan et al., 2010, 2012). Behavioral and electrographic changes in $CAR^{-/-}$ mice may be sustained by constitutive neuro-vascular defects. The exact cellular pathological pathways involved in the behavioral and morphological changes observed $CAR^{-/-}$ mice remains to be investigated.

Supplementary Material

Refer to Web version on PubMed Central for supplementary material.

Acknowledgements

We would like to thank Emmanuel Valjent for the significant discussion and sharing equipment used for the behavioral tests. We would like to thank Xavier DeCleves for kindly sharing his know-how on brain microvessel isolation. Finally, we thank Chrystel Lafont for the 2-photon images acquisition.

Supported by NIH R01 NS078307, FFRE-TF1, FFRE Prix Valerie Chamaillard and Fondation Française pour la Recherche sur l'Épilepsie. IPAM imaging Platform (IGF) and electron Microscopy Platform (UM).

References

Abbott NJ, Ronnback L, Hansson E, 2006 Astrocyte–endothelial interactions at the blood–brain barrier. Nat. Rev. Neurosci 7, 41–53. [PubMed: 16371949]

Banerjee M, Robbins D, Chen T, 2015 Targeting xenobiotic receptors PXR and CAR in human diseases. Drug Discov. Today 20, 618–628. [PubMed: 25463033]

Bauer B, Yang XD, Hartz AMS, Olson ER, Zhao R, Kalvass JC, et al., 2006 In vivo activation of human pregnane X receptor tightens the blood–brain barrier to methadone through P-glycoprotein up-regulation. Mol. Pharmacol 70, 1212–1219. [PubMed: 16837625]

Chakraborty S, Kanakasabai S, Bright JJ, 2011 Constitutive androstane receptor agonist CITCO inhibits growth and expansion of brain tumour stem cells. Br. J. Cancer 104, 448–459. [PubMed: 21224854]

Chauviere L, Rafrafi N, Thinus-Blanc C, Bartolomei F, Esclapez M, Bernard C, 2009 Early deficits in spatial memory and theta rhythm in experimental temporal lobe epilepsy. J. Neurosci 29, 5402–5410. [PubMed: 19403808]

Cherian MT, Lin W, Wu J, Chen T, 2015a CINPA1 is an inhibitor of constitutive androstane receptor that does not activate pregnane X receptor. Mol. Pharmacol 87, 878–889. [PubMed: 25762023]

Cherian MT, Chai SC, Chen T, 2015b Small-molecule modulators of the constitutive androstane receptor. Expert Opin. Drug Metab. Toxicol 11, 1099–1114. [PubMed: 25979168]

Dai YB, Tan XJ, Wu WF, Warner M, Gustafsson JA, 2012 Liver X receptor beta protects dopaminergic neurons in a mouse model of Parkinson disease. Proc. Natl. Acad. Sci. U. S. A 109, 13112–13117. [PubMed: 22826221]

Falcone T, Janigro D, Lovell R, Simon B, Brown CA, Herrera M, et al., 2015 S100B blood levels and childhood trauma in adolescent inpatients. J. Psychiatr. Res 62, 14–22. [PubMed: 25669696]

Fan X, Kim HJ, Bouton D, Warner M, Gustafsson JA, 2008 Expression of liver X receptor beta is essential for formation of superficial cortical layers and migration of later-born neurons. Proc. Natl. Acad. Sci. U. S. A 105, 13445–13450. [PubMed: 18768805]

Friedman A, 2011 Blood–brain barrier dysfunction, status epilepticus, seizures, and epilepsy: a puzzle of a chicken and egg? Epilepsia 52 (Suppl. 8), 19–20. [PubMed: 21967353]

Frye CA, Koonce CJ, Walf AA, 2013 Pregnane xenobiotic receptors and membrane progestin receptors: role in neurosteroid-mediated motivated behaviours.J. Neuroendocrinol 25, 1002–1011. [PubMed: 24028379]

Gangarossa G, Ceolin L, Paucard A, Lerner-Natoli M, Perroy J, Fagni L, et al., 2014a Repeated stimulation of dopamine D1-like receptor and hyperactivation of mTOR signaling lead to generalized seizures, altered dentate gyrus plasticity, and memory deficits. Hippocampus 24, 1466–1481. [PubMed: 25044816]

Gangarossa G, Laffray S, Bourinet E, Valjent E, 2014b T-type calcium channel Cav3.2 deficient mice show elevated anxiety, impaired memory and reduced sensitivity to psychostimulants. Front. Behav. Neurosci 8, 92. [PubMed: 24672455]

Hawk JD, Bookout AL, Poplawski SG, Bridi M, Rao AJ, Sulewski ME, et al., 2012 NR4A nuclear receptors support memory enhancement by histone deacetylase inhibitors. J. Clin. Invest 122, 3593–3602. [PubMed: 22996661]

Huang F, Wang T, Lan Y, Yang L, Pan W, Zhu Y, et al., 2015 Deletion of mouse FXR gene disturbs multiple neurotransmitter systems and alters neurobehavior. Front. Behav. Neurosci 9, 70. [PubMed: 25870546]

Kaur P, Sodhi RK, 2015 Memory recuperative potential of rifampicin in aluminum chloride-induced dementia: Role of pregnane X receptors. Neuroscience 288, 24–36. [PubMed: 25545714]

Ke MT, Fujimoto S, Imai T, 2013 SeeDB: a simple and morphology-preserving optical clearing agent for neuronal circuit reconstruction. Nat. Neurosci 16, 1154–1161. [PubMed: 23792946]

Khandaker GM, Cousins L, Deakin J, Lennox BR, Yolken R, Jones PB, 2015 Inflammation and immunity in schizophrenia: implications for pathophysiology and treatment. Lancet Psychiatry 2, 258–270. [PubMed: 26359903]

Kleefstra T, Kramer JM, Neveling K, Willemsen MH, Koemans TS, Vissers LE, et al., 2012 Disruption of an EHMT1-associated chromatin-modification module causes intellectual disability. Am. J. Hum. Genet 91, 73–82. [PubMed: 22726846]

Li D, Mackowiak B, Brayman TG, Mitchell M, Zhang L, Huang SM, et al., 2015 Genome-wide analysis of human constitutive androstane receptor (CAR) transcriptome in wild-type and CAR-knockout HepaRG cells. Biochem. Pharmacol 98, 190–202. [PubMed: 26275810]

Litwa E, Rzemieniec J, Wnuk A, Krzeptowski W, Lason W, Kajta M, 2015 RXRalpha, PXR and CAR xenobiotic receptors mediate the apoptotic and neurotoxic actions of nonylphenol in mouse hippocampal cells. J. Steroid Biochem. Mol. Biol

Marchi N, Angelov L, Masaryk T, Fazio V, Granata T, Hernandez N, et al., 2007 Seizure-promoting effect of blood–brain barrier disruption. Epilepsia 48, 732–742. [PubMed: 17319915]

Marchi N, Granata T, Ghosh C, Janigro D, 2012 Blood–brain barrier dysfunction and epilepsy: pathophysiologic role and therapeutic approaches. Epilepsia 53, 1877–1886. [PubMed: 22905812]

Marchi N, Granata T, Janigro D, 2014 Inflammatory pathways of seizure disorders.Trends Neurosci 37, 55–65. [PubMed: 24355813]

Obermeier B, Daneman R, Ransohoff RM, 2013 Development, maintenance and disruption of the blood–brain barrier. Nat. Med 19, 1584–1596. [PubMed: 24309662]

Ogura J, Terada Y, Tsujimoto T, Koizumi T, Kuwayama K, Maruyama H, et al., 2012 The decrease in farnesoid X receptor, pregnane X receptor and constitutive androstane receptor in the liver after intestinal ischemia-reperfusion. J. Pharm. Pharm. Sci 15, 616–631. [PubMed: 23331901]

Roques BB, Leghait J, Lacroix MZ, Lasserre F, Pineau T, Viguie C, et al., 2013 The nuclear receptors pregnane X receptor and constitutive androstane receptor contribute to the impact of fipronil on hepatic gene expression linked to thyroid hormone metabolism. Biochem. Pharmacol 86, 997–1039. [PubMed: 23962444]

Ross J, Plummer SM, Rode A, Scheer N, Bower CC, Vogel O, et al., 2010 Human constitutive androstane receptor (CAR) and pregnane X receptor (PXR) support the hypertrophic but not the hyperplastic response to the murine nongenotoxic hepatocarcinogens phenobarbital and chlordane in vivo. Toxicol. Sci 116, 452–466. [PubMed: 20403969]

Shawahna R, Uchida Y, Decleves X, Ohtsuki S, Yousif S, Dauchy S, et al., 2011 Transcriptomic and quantitative proteomic analysis of transporters and drug metabolizing enzymes in freshly isolated human brain microvessels. Mol. Pharm 8, 1332–1341. [PubMed: 21707071]

Snyder HM, Corriveau RA, Craft S, Faber JE, Greenberg SM, Knopman D, et al., 2015 Vascular contributions to cognitive impairment and dementia including Alzheimer's disease. Alzheimers Dement 11, 710–717. [PubMed: 25510382]

Tan XJ, Fan XT, Kim HJ, Butler R, Webb P, Warner M, et al., 2010 Liver X receptor beta and thyroid hormone receptor alpha in brain cortical layering. Proc. Natl. Acad. Sci. U. S. A 107, 12305–12310. [PubMed: 20566868]

Tan XJ, Dai YB, Wu WF, Warner M, Gustafsson JA, 2012 Anxiety in liver X receptor beta knockout female mice with loss of glutamic acid decarboxylase in ventromedial prefrontal cortex. Proc. Natl. Acad. Sci. U. S. A 109, 7493–7498. [PubMed: 22529354]

Thorsell A, Michalkiewicz M, Dumont Y, Quirion R, Caberlotto L, Rimondini R, et al., 2000 Behavioral insensitivity to restraint stress, absent fear suppression of behavior and impaired spatial learning in transgenic rats with hippocampal neuropeptide Y overexpression. Proc. Natl. Acad. Sci. U. S. A 97, 12852–12857. [PubMed: 11058155]

Thorsell A, Karlsson RM, Heilig M, 2006 NPY in alcoholism and psychiatric disorders.EXS 183–192. [PubMed: 16383007]

Tolson AH, Wang H, 2010 Regulation of drug-metabolizing enzymes by xenobiotic receptors: PXR and CAR. Adv. Drug Deliv. Rev 62, 1238–1249. [PubMed: 20727377]

van Vliet EA, Otte WM, Gorter JA, Dijkhuizen RM, Wadman WJ, 2014 Longitudinal assessment of blood–brain barrier leakage during epileptogenesis in rats. A quantitative MRI study. Neurobiol. Dis 63, 74–84. [PubMed: 24321435]

Venkatesh M, Mukherjee S, Wang H, Li H, Sun K, Benechet AP, et al., 2014 Symbiotic bacterial metabolites regulate gastrointestinal barrier function via the xenobiotic sensor PXR and Toll-like receptor 4. Immunity 41, 296–310. [PubMed: 25065623]

Wang XQ, Sykes DB, Miller DS, 2010 Constitutive androstane receptor-mediated up-regulation of ATP-driven xenobiotic efflux transporters at the blood–brain barrier. Mol. Pharmacol 78, 376–383. [PubMed: 20547735]

Wang X, Fang X, Zhou J, Chen Z, Zhao B, Xiao L, et al., 2013 Shear stress activation of nuclear receptor PXR in endothelial detoxification. Proc. Natl. Acad. Sci. U. S. A 110, 13174–13179. [PubMed: 23878263]

Wang SL, Lei T, Zhang K, Zhao WX, Fang L, Lai BC, et al., 2014 Xenobiotic pregnane X receptor (PXR) regulates innate immunity via activation of NLRP3 inflammasome in vascular endothelial cells. J. Biol. Chem 289, 30075–30081. [PubMed: 25202020]

Wei P, Zhang J, Egan-Hafley M, Liang S, Moore DD, 2000 The nuclear receptor CAR mediates specific xenobiotic induction of drug metabolism. Nature 407, 920–923. [PubMed: 11057673]

Wilhelmsson U, Bushong EA, Price DL, Smarr BL, Phung V, Terada M, et al., 2006 Redefining the concept of reactive astrocytes as cells that remain within their unique domains upon reaction to injury. Proc. Natl. Acad. Sci. U. S. A 103, 17513–17518. [PubMed: 17090684]

Yang H, Wang H, 2014 Signaling control of the constitutive androstane receptor (CAR). Protein Cell 5, 113–123. [PubMed: 24474196]

Zhao Y, Bruemmer D, 2010 NR4A orphan nuclear receptors: transcriptional regulators of gene expression in metabolism and vascular biology. Arterioscler. Thromb. Vasc. Biol 30, 1535–1541. [PubMed: 20631354]

Zhao Y, Howatt DA, Gizard F, Nomiyama T, Findeisen HM, Heywood EB, et al., 2010 Deficiency of the NR4A orphan nuclear receptor NOR1 decreases monocyte adhesion and atherosclerosis. Circ. Res 107, 501–511. [PubMed: 20558821]

Zhao Z, Nelson AR, Betsholtz C, Zlokovic BV, 2015 Establishment and dysfunction of the blood–brain barrier. Cell 163, 1064–1078. [PubMed: 26590417]

Zhou C, Verma S, Blumberg B, 2009 The steroid and xenobiotic receptor (SXR), beyond xenobiotic metabolism. Nucl. Recept. Signal 7, e001. [PubMed: 19240808]

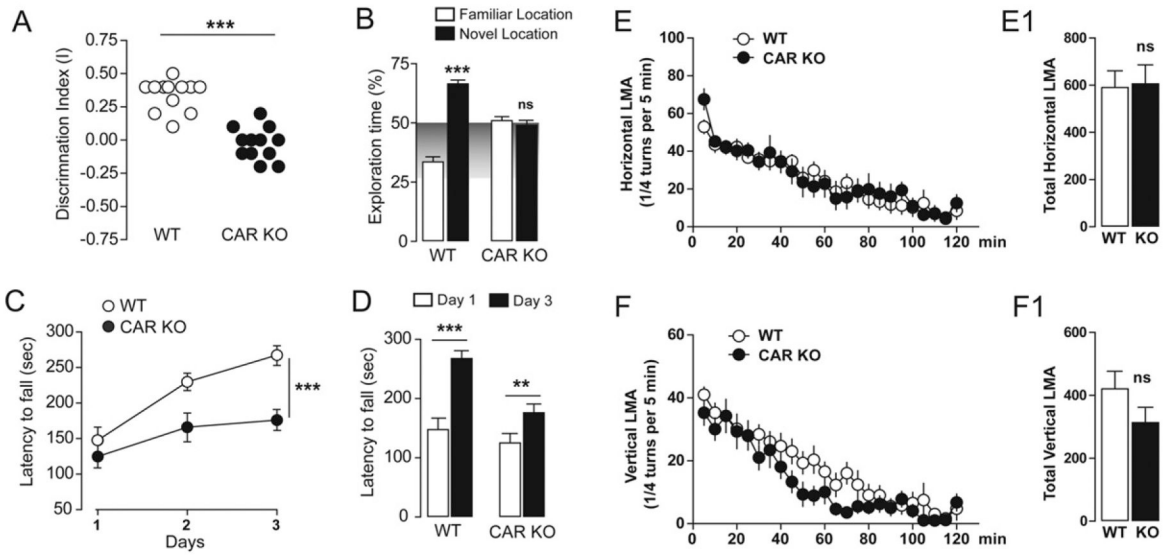

Fig. 1.

Memory and motor functions in CAR$^{-/-}$ mice. A) Discrimination index in CAR$^{-/-}$ mice (spatial object recognition test). Data (means ± SEM) were analyzed using one-way ANOVA: $F_{(2, 35)} = 20.85$, *** $P < 0.001$. B) Time of exploration of the novel location in CAR$^{-/-}$ mice. Data were analyzed using two-way ANOVA: (Object exploration × Genotype: $F_{(2, 66)} = 36.77$, $P < 0.0001$). Specific comparisons: *** $P < 0.001$ (WT-new vs WT-familiar). C) Coordination and motor learning over a training period of 3 days in CAR$^{-/-}$ mice (rotarod). Data were analyzed using two-way ANOVA (Time × Genotype: $F_{(4, 66)} = 1.93$, $P = 0.11$; Time: $F_{(2, 66)} = 25.67$, $P < 0.0001$; Genotype: $F_{(2, 66)} = 15.63$, $P < 0.0001$). Specific comparisons: ***$P < 0.001$ (CAR KO-Day3 vs WT-Day3). D) Specific comparison of motor learning in WT (n = 12) and CAR KO (n = 12) at day 3. Data were analyzed using within *t*-test. Specific comparisons: *** $P < 0.001$ (WT-Day3 vs WT-Day1) and ** $P < 0.01$ (CAR KO-Day3 vs CAR KO-Day1). E–F) Spontaneous horizontal and vertical (rearing) locomotor activity in CAR$^{-/-}$ mice (novel non-stressful environment). Data were analyzed using two-way ANOVA: (Time × Genotype: $F_{(46, 528)} = 0.79$, $P = 0.83$; Time: $F_{(23, 528)} = 20.01$, $P < 0.0001$; Genotype: $F_{(2, 528)} = 33.89$, $P < 0.0001$) (E). Data were analyzed using two-way ANOVA: (Time × Genotype: $F_{(46, 528)} = 0.76$, $P = 0.88$; Time: $F_{(23, 528)} = 34.64$, $P < 0.0001$; Genotype: $F_{(2, 528)} = 18.94$, $P < 0.0001$) (F). (E1 and F1) Histograms show cumulative activities. Student's *t*-test: $P > 0.05$, ns.

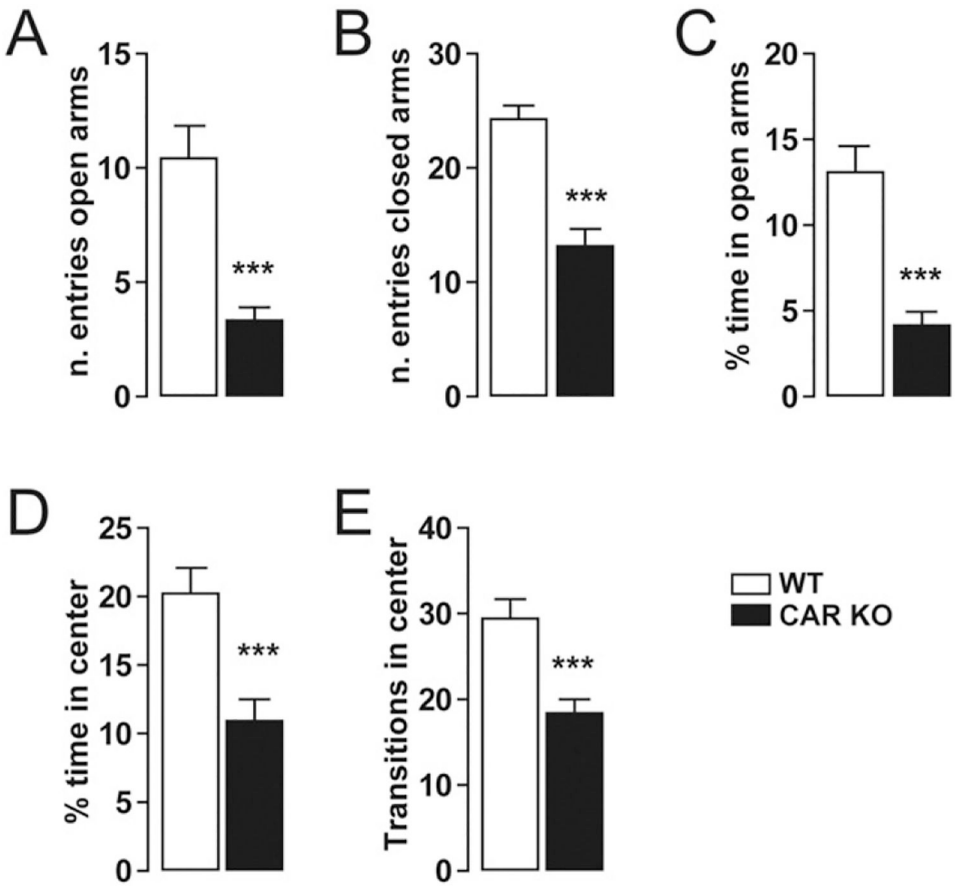

Fig. 2.

Anxiety-like behavior in CAR deficient mice. (A–B) Histograms indicate the number of entries of CAR KO (n = 12) and WT mice (n = 12) in the open and closed arms of the EPM. (C) Histograms show the percentage of time CAR KO (n = 12) and WT mice (n = 12) spent in the open arms. (D) Histograms show the percentage of time CAR KO (n = 12) and WT mice (n = 12) spent in the center zone of the open field. (E) Histograms indicate the number of transitions CAR KO (n = 12) and WT mice (n = 12) made in the center zone of the open field. All data (means ± SEM) were analyzed using Student's t-test: *** $P < 0.001$.

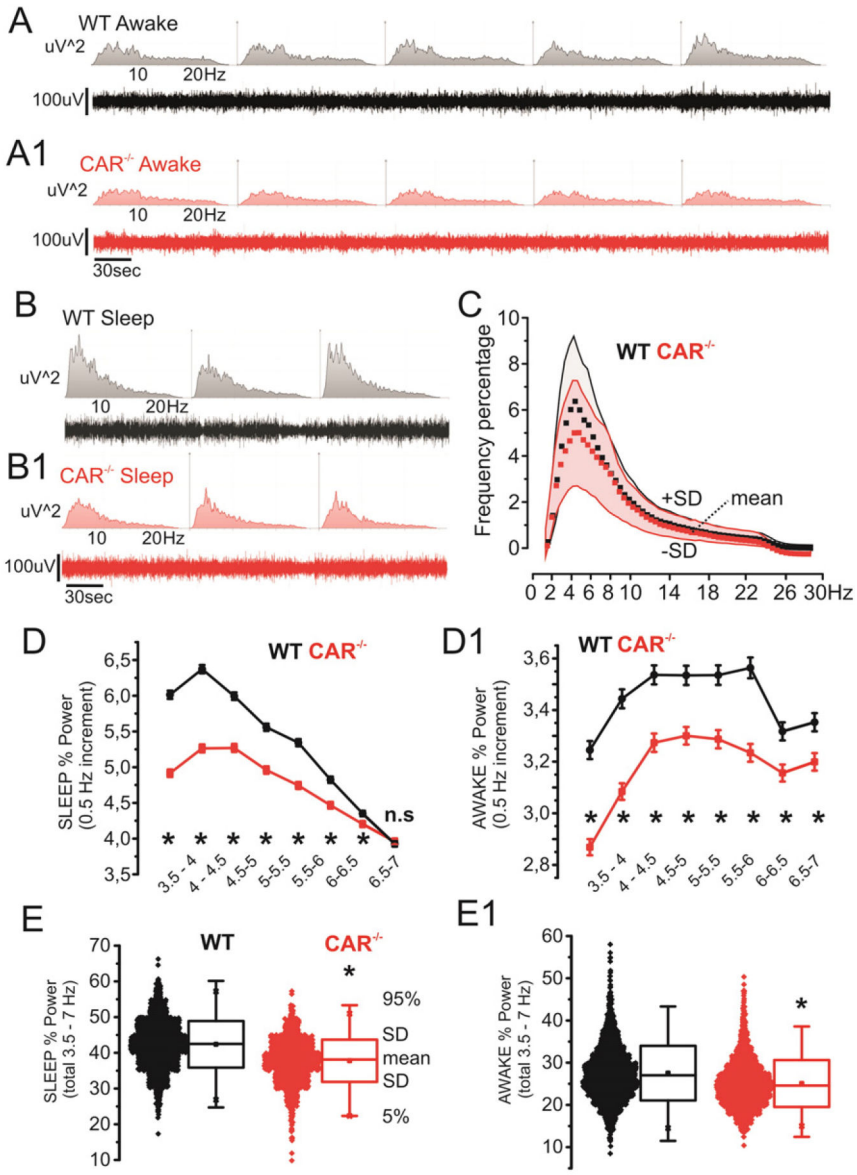

Fig. 3.

Decreased 3.5–7 Hz activity in CAR$^{-/-}$ mice. A–B) Examples of EEG and correspondent spectrogram (WT and CAR$^{-/-}$, awake/exploration and sleep; 0–30 Hz). C) Relative power (percentage; n = 4 mice/group) shows a decrease in the 3.5–7 hertz range (red = CAR$^{-/-}$, grey = WT; data points and shadows indicate mean ± SD respectively). D-D1) detailed frequency analysis (0.5 Hz increment) relative to sleep and awake/exploration stages. E-E1) Representation of D-D1 data accumulation (see Section 2 for details).

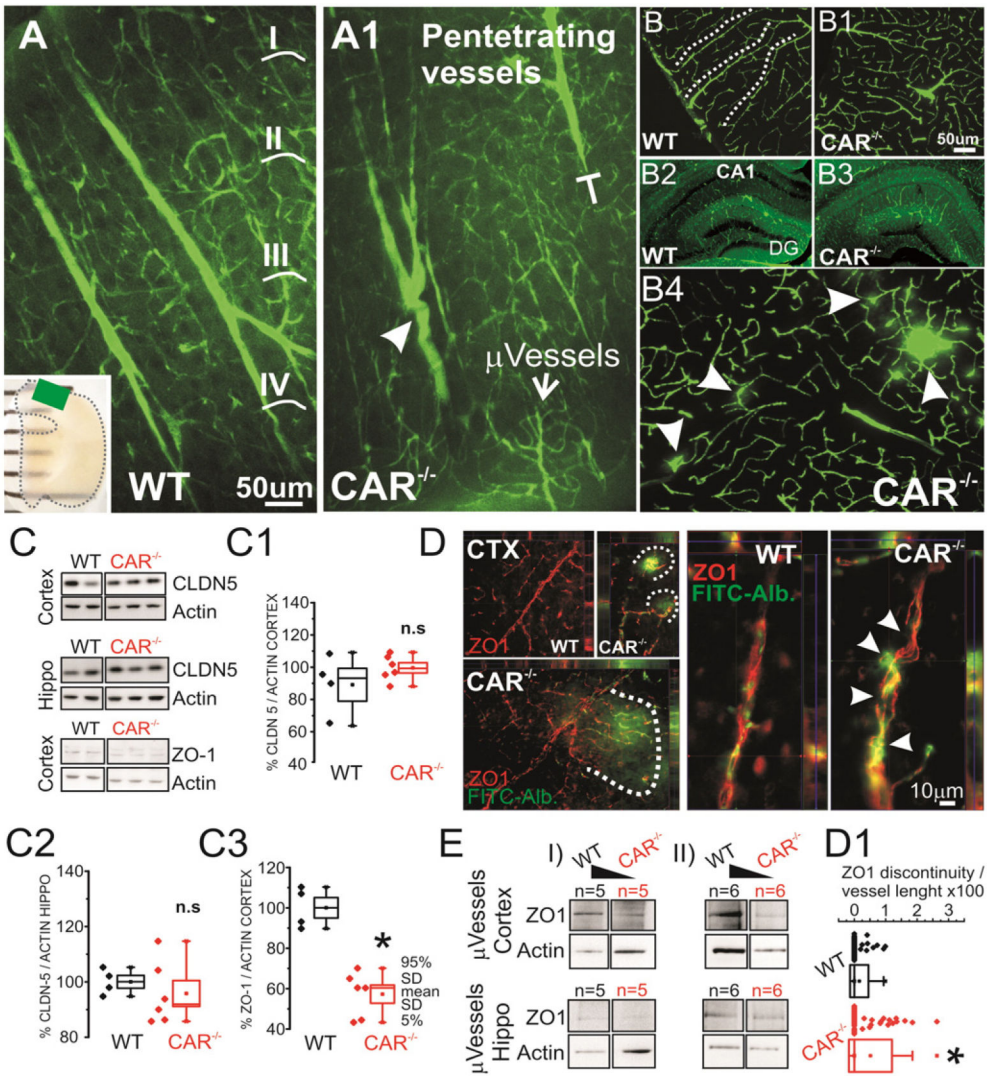

Fig. 4.

Cerebrovascular morphology and tight junction expression in $CAR^{-/-}$ mice. A-A1) 2-Photon images obtained from SeeDB transparent brain preparations (ROI in the insert). Irregular penetrating cortical vessels (corresponding to layers I–IV) were found in $CAR^{-/-}$ as compared to WT mice (t-shape line and arrowhead). See Supplemental Movies 1 and 2. B–B1) Differential patterns of $FITC^{+}$ penetrating (dotted lines) in WT vs $CAR^{-/-}$ mice. B2–B3) At the macroscopic level hippocampal microvessel anatomy was not affected. See Supplemental Fig. 2 for quantifications. B4) Example of localized microvascular permeability visualized using FITC leakages (arrows). C-C3) Decreased ZO1 expression and not CLDN-5 in total brain tissues. D) Immunohistochemistry displaying point form FITC-albumin leakages (dotted lines) consistent with discontinuous Z01 lining. An example is provided (arrowheads). D1) Quantification of ZO1 discontinuity on FITC-Albumin microvessels. Each data point refers to one vessel. See Section 2 for details. E) ZO1 decreased in isolated hippocampal and cortical brain microvessels of $CAR^{-/-}$ mice. Inserts i) and ii) refer to two separate experiments where a total of n = 10 and n = 12 mice were used.

N refers to the number of mice that were pulled together obtaining one corresponding WB band.

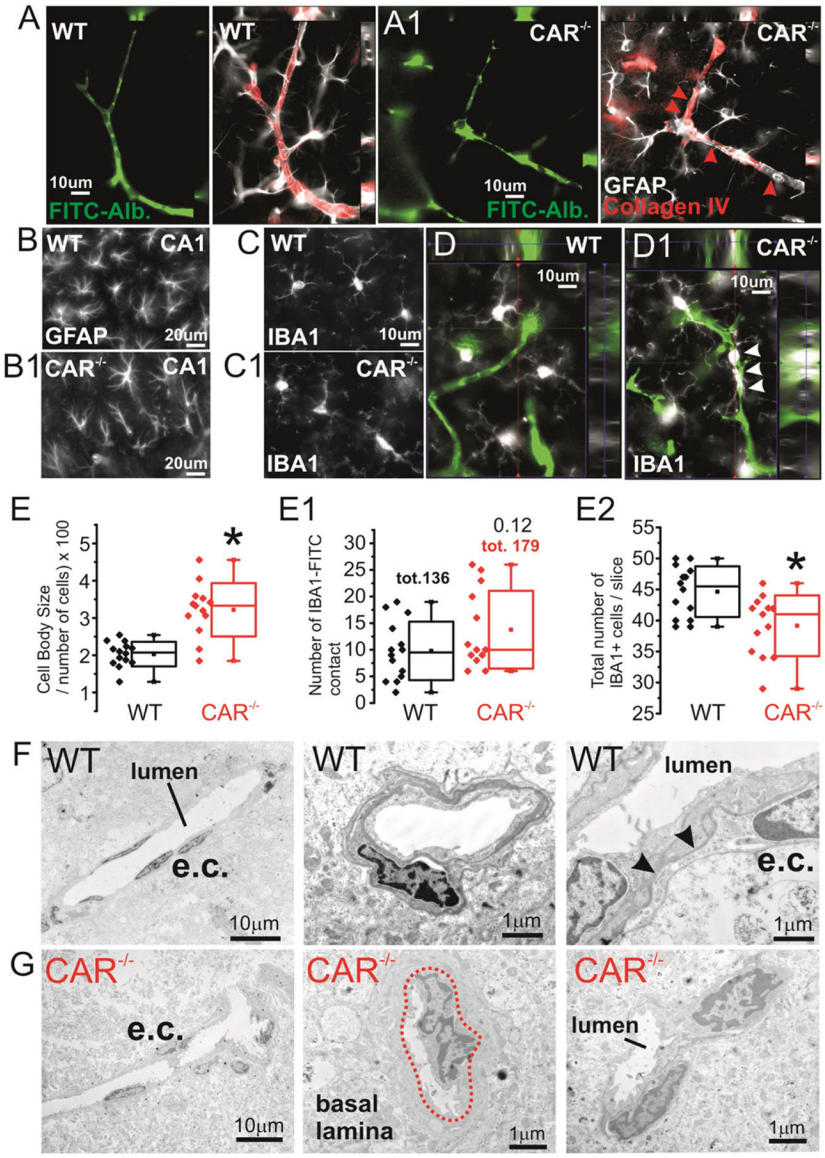

Fig. 5.

Signs of parenchymal cell changes in CAR$^{-/-}$ mice. A-A1) Collagen IV immunoreactivity and astrocyte end-feet consistently define FITC-albumin microvessels in WT mice. B-B1) Presence of hippocampal GFAP morphological changes and C–D) perivascular (white arrowheads) IBA^{+} cells. E-E1) Quantification indicates increase in cell body size, a trend increase in the number of IBA1^{+} ramifications lining the microvessels but a decrease in the number of IBA1^{+} cells. F–G) Although not widespread, microvascular changes in CAR$^{-/-}$ mice also included: i) dishomogenous cellular (e.c. left panels) distribution around the lumen, ii) basal lamina remodeling (central panels) and iii) irregular cell-to-cell contact (right panels).

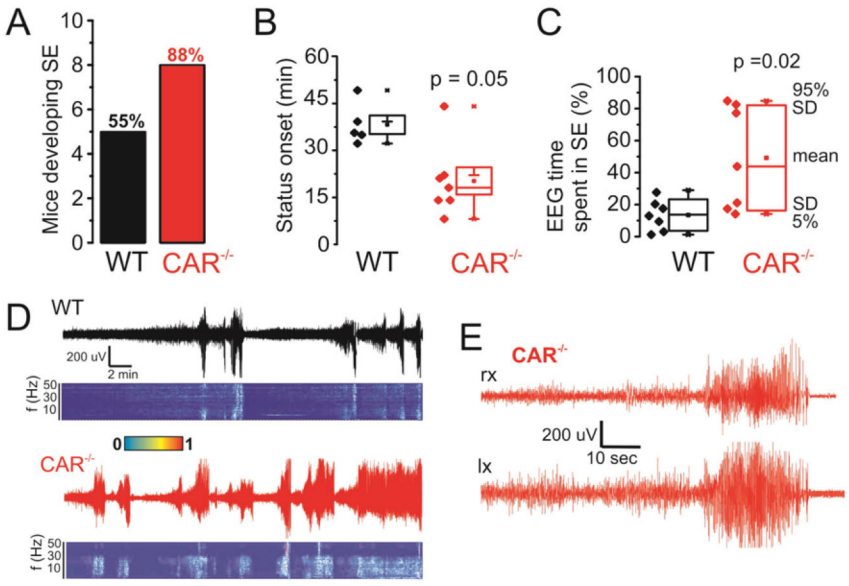

Fig. 6.

$CAR^{-/-}$ are more susceptible to systemic KA as compared to WT. A–C) $CAR^{-/-}$ mice rapidly developed status epilepticus (SE) after i.p. KA. Video-EEG confirmed $CAR^{-/-}$ mice susceptibility to KA as indicated by increased EEG % time spent in SE (see Section 2). D–E) Examples (SE) of EEG and time-joint frequency analysis observed WT and $CAR^{-/-}$ mice.